

Generalized quantum measurements with matrix product states: Entanglement phase transition and clusterization

Elmer V. H. Doggen,^{1,2,*} Yuval Gefen,³ Igor V. Gornyi,^{1,2,4} Alexander D. Mirlin,^{1,2,5,6} and Dmitry G. Polyakov¹

¹*Institute for Quantum Materials and Technologies, Karlsruhe Institute of Technology, 76021 Karlsruhe, Germany*

²*Institut für Theorie der Kondensierten Materie, Karlsruhe Institute of Technology, 76128 Karlsruhe, Germany*

³*Department of Condensed Matter Physics, Weizmann Institute of Science, 7610001 Rehovot, Israel*

⁴*Ioffe Institute, 194021 St. Petersburg, Russia*

⁵*Petersburg Nuclear Physics Institute, 188300 St. Petersburg, Russia*

⁶*Landau Institute for Theoretical Physics, 119334 Moscow, Russia*

(Dated: July 26, 2021)

We propose a method, based on matrix product states, for studying the time evolution of many-body quantum lattice systems under continuous and site-resolved measurement. Both the frequency and the strength of generalized measurements can be varied within our scheme, thus allowing us to explore the corresponding two-dimensional phase diagram. The method is applied to one-dimensional chains of nearest-neighbor interacting hard-core bosons. A transition from an entangling to a disentangling (area-law) phase is found. However, by resolving time-dependent density correlations in the monitored system, we find important differences between different regions at the phase boundary. In particular, we observe a peculiar phenomenon of measurement-induced particle clusterization that takes place only for frequent moderately strong measurements, but not for strong infrequent measurements.

I. INTRODUCTION

Open quantum systems [1, 2] form the bridge between the world of unitary, deterministic evolution of closed quantum systems [3], and the familiar experience of our macroscopic world. Recently, open quantum systems have received renewed interest in the context of quantum information processing and quantum circuits. The coupling to the environment can lead to decoherence in arrays of qubits, which limits the fidelity of quantum operations. A sufficiently high fidelity is essential for the performance of programmable quantum devices, in particular for “quantum supremacy,” which was reported to have been achieved recently [4].

Quantum measurements, via their back-action on the measured system, can mimic the effect of an environment. In a sense, the environment also “measures” the system, but without “recording” the extracted information. To that effect, coupling to the environment is a special type of “blind measurement” [5]. Designing specific measurement protocols can be considered as engineering of the environment to which the quantum system is coupled. Improving our understanding of quantum measurement processes is therefore of immediate practical importance. At the same time, controlling the decoherence induced by the coupling to the environment may also help to advance our fundamental understanding of quantum measurements [6, 7].

This important role of measurements in the quantum-information context, as well as their relation to decoherence and entanglement spreading [8–10], has led to a flurry of activity on the subject, especially with regard

to entanglement transitions using a quantum circuit description [11–28]. The effect of local quantum measurements on entanglement has also been considered for systems described by a lattice Hamiltonian, in particular, for many-body localized systems [29], the quantum Ising chain [30–33], non-interacting spinless fermionic models [34–36], Hubbard-type interacting chains with short-range [37] and long-range [38] interactions, and ultracold gases [39]. The question as to whether the effect of measurements on quantum circuits is qualitatively the same for real many-body systems is a subject of ongoing studies, as we detail below.

A key feature that has emerged in the pioneering studies of monitored systems is the interplay between the entangling effect of time evolution and the disentangling effect of the measurement, leading to an entanglement phase transition [11–14]. Various types of measurements have been considered: local projective measurements, local weak measurements that only slightly perturb the system (for their recent applications in other contexts, see, e.g., Refs. [5, 40–49]), non-local measurements of several sites of the system, and global measurements that act on the many-body system as a whole. The main diagnostic tool for the measurement-induced entanglement transition is the behavior of the entanglement entropy averaged over the measurement runs, but other indicators, such as mutual information or entanglement negativity, have also been used to explore the phenomenon. However, manifestations of the entanglement phase transition in more conventional density correlations are not yet sufficiently explored.

The entanglement transition was discussed for measurement-only dynamics, where non-local measurements produce both entangling (by non-locality) and disentangling (by projection) trends [26, 50]. The measurement-induced transition was argued to be related

* Corresponding author: elmer.doggen@kit.edu

to the “purification transition” [18], which can be employed for quantum-state preparation, control, and manipulation by means of quantum measurements. In addition, the properties of the entanglement transition have been linked to the theory of error corrections in quantum information processing [21, 22, 26, 28, 51–53]. In the presence of additional symmetries and constraints, a more sophisticated phase diagram may emerge, where the entanglement transition is accompanied by other types of phase transitions, see, e.g., Refs. [24, 54].

A key open question concerns the degree of universality between the various types of measurement protocols, applied to various different types of systems. In particular, it has been argued [16, 17] that the effect of continuous (weak, or “generalized”) quantum measurements on quantum circuits is, by and large, analogous to the effect of rare projective measurements. A generalized phase diagram of hybrid quantum circuits in the plane of frequency vs. strength of measurements was analyzed in Refs. [15, 16], where a transition between entangling (for weak or infrequent measurements) and disentangling (strong or frequent) phases was established. At the same time, indications of a possible essential difference between the transitions at strong and weak measurements were reported in Ref. [15]. Thus, it remains a challenging task to explore the universality of the entanglement transition for various measurement setups.

Another important—and still open—question concerns the properties of different phases around the transition. The scaling of entanglement entropy with the system size exactly at the entanglement transition has been argued to exhibit logarithmic behavior [23, 55] familiar from models described by conformal field theory [8, 10, 56]. On the entangling side of the transition, volume-law scaling was found in various hybrid unitary circuits, whereas in continuously monitored fermionic and spin systems both volume-law and logarithmic-law [33, 35–37, 57] types of entangling scaling were reported. Such entangled phases were argued [34] to be unstable to arbitrarily weak measurements in the case of continuously monitored non-interacting fermionic chains that are measured at all sites. The logarithmic scaling corresponds to the emergence of a critical entangled steady state in the thermodynamic limit, while the properties of small-size systems would correspond to volume-law behavior [35, 36]. A critical phase characterized by the conformal scaling of observables was found in free models subject to non-unitary evolution governed by a non-Hermitian Hamiltonian [23, 58].

One difficulty in determining the degree of universality in this large array of different systems, however, is that numerical studies thus far have mostly focused on fine-tuned models and not generic many-body systems. This means that, for instance, the role of interactions between particles, integrability of the model, as well as the interplay between many-body and the measurement-induced effects are largely unclear. Another natural deficiency of numerical studies of the measurement-induced transi-

tions in correlated many-body systems is a limited accessibility of large system sizes, which is especially crucial for exploring the predicted change of the behavior [35] with increasing system size in the entangling phase.

A particularly promising direction, therefore, is to use the versatile approach of matrix product states (MPS) [59, 60] to simulate the dynamics, as applied recently to quantum measurements [39, 50, 61]. Specifically, MPS are a class of variational Ansätze that approximate the exponential complexity of generic many-body states through a polynomial number of parameters, restricted to low- to moderately-entangled states.

In the present paper, we propose an MPS-based approach that describes quantum measurements in a continuous way. The dynamics of the monitored system is represented by the combination of unitary (governed by a many-body Hamiltonian) and stochastic non-unitary (effective non-Hermitian Hamiltonian) evolution. The latter models a local coupling to external degrees of freedom, thus bridging the concepts of environment-induced decoherence and quantum measurements. The advantage of the protocol we will formulate here is that it can be applied to any problem that permits an MPS description and hence includes interacting models. Importantly, the MPS approach can be controllably used for interacting many-body models with system sizes considerably larger than those accessible to exact methods, which are restricted to ≈ 20 lattice sites.

The model we consider here is an interacting many-body system of hard-core bosons on a lattice, which constitutes a Luttinger liquid in the low-energy, continuum limit. We study the measurement-induced dynamics starting from the (moderately entangled) ground state of the system. Depending on the strength and frequency (probability) of the measurement process, the dynamics is either entangling or disentangling, in agreement with recent predictions based on the aforementioned quantum circuit descriptions. However, we also uncover a distinct feature of the system under study: in a certain parameter range near the transition between the entangling and disentangling phases, a clustering of particles occurs such that extended regions of particles and holes emerge over time. This signifies that, while the overall phase diagram breaks down into two distinct phases according to the entanglement scaling, the properties of the phases and the transition between them, quantified in other observables, depend on the measurement implementation.

The paper is organized as follows. In Sec. II, we specify the system Hamiltonian and introduce the local measurements through a stochastic non-unitary evolution. We also compare our implementation of measurements with the existing approaches. In Sec. III, we introduce the observables that we numerically calculate using the MPS and describe the simulation results. The obtained results for the entanglement entropy and density correlations are discussed in terms of the “phase diagrams” in Sec. IV. Finally, we summarize our findings in Sec. V.

II. MODEL AND METHOD

A. System

We consider a hard-core boson model on a lattice of length L (sites $x = 1, 2, \dots, L$) characterized by the following Hamiltonian:

$$\mathcal{H}_0 = \sum_{x=1}^{L-1} \left[-\frac{J}{2} \left(\hat{b}_x^\dagger \hat{b}_{x+1} + \text{H.c.} \right) + \Delta \hat{n}_x \hat{n}_{x+1} \right]. \quad (1)$$

Here $\hat{b}_x^\dagger, \hat{b}_x$ are the bosonic creation and annihilation operators and $\hat{n}_x \equiv \hat{b}_x^\dagger \hat{b}_x$ on the $\{0, 1\}$ -manifold of local occupation. We set $J = 1$ and $\hbar = 1$. For $|\Delta| \leq 1$, the ground state is a Luttinger liquid (otherwise, it is ferro- or antiferromagnetic). Below, we focus on this range of interaction, choosing (for the most part of the paper, except for a brief discussion of other values of Δ in Sec. IV B 2) attractive interaction with $\Delta = -0.5$. The model (1) is known as the t - V model in the spinless fermion language and the XXZ Heisenberg chain in the spin-1/2 language. Throughout the paper, we consider the case of half-filling; namely, we take L to be even and fix the number of particles to be $L/2$.

B. Measurement

We break the time axis into measurement intervals of the same duration T , i.e., the j -th measurement occurs between the times t_j and $t_{j+1} = t_j + T$. The measurement in the j -th interval is implemented as a two-component process: (i) a quantum quench by adding at time t_j and removing at time t_{j+1} a random purely imaginary (anti-Hermitian) on-site potential $\mathcal{H}_{\text{meas}}^j$ to the Hamiltonian \mathcal{H}_0 and (ii) a continuous—between t_j and t_{j+1} —restoration of the wave function norm through a global renormalization of the MPS. Specifically, $\mathcal{H}_{\text{meas}}^j$ is of the form

$$\mathcal{H}_{\text{meas}}^j = -iM \sum_x p_x^j \text{sgn}(n_x - m_x^j) \hat{n}_x, \quad (2)$$

where $n_x \equiv \langle \hat{n}_x \rangle$ is the expectation value of the on-site density, $p_x^j = \{0, 1\}$ is a binary random variable with values 0 and 1, and $m_x^j \in (0, 1)$ is a random variable uniformly distributed between 0 and 1. The constant M is real and positive.

The quantity p_x^j indicates whether the measurement is performed at the site x within the j -th time interval. Its stochastic distribution is characterized by the probability P_x^j that the site x is measured at the j -th time step (which corresponds to $p_x^j = 1$). In this paper, we take P_x^j to be time independent and the same over all lattice sites, with $P_x^j \equiv P$. The value of P thus parameterizes the measurement rate, with $P = 1$ describing the limit of frequent measurements at each time step.

The probabilistic character of quantum-measurement outcomes is enforced by the randomness of the quantity m_x^j . The stochastic behavior of the factor $\text{sgn}(n_x - m_x^j)$, which depends on n_x , is then akin to the Born rule. In the limiting cases of $n_x = 1$ and 0 at a given time, the sign function is equal to 1 in the former case and -1 in the latter, irrespective of m_x^j , which corresponds to deterministically measuring the presence ($n_x = 1$) or absence ($n_x = 0$) of a particle. For intermediate values of n_x , the measurement outcome is probabilistic, depending on both n_x and the random choice of m_x^j .

The quantity M characterizes the measurement strength. The limit of $MT \gg 1$ describes a projective measurement of the particle density, whereas the opposite limit corresponds to a weak measurement. Indeed, our implementation of the measurement can be formalized in terms of a sequence of imaginary-time evolution events governed by $\mathcal{H}_{\text{meas}}^j$, superimposed onto the real-time evolution induced by \mathcal{H}_0 . The two types of dynamics compete with each other as far as the density distribution in space is concerned. The unitary dynamics drives the system towards a spatially homogeneous state with a local occupancy of $1/2$. By contrast, a fast, corresponding to large M , imaginary-time dynamics at a given site drives the local occupancy to either fully occupied or fully empty, thus embodying the notion of a projective measurement.

Consecutive measurements describe a Markovian process, with $\mathcal{H}_{\text{meas}}^{j+1}$ at step $j+1$ characterized by a randomly chosen set of p_x^{j+1} and m_x^{j+1} , which is independent of p_x^j and m_x^j , and the running value of the expectation value n_x . As already mentioned above, the latter evolves in time under the action of both the Hermitian and anti-Hermitian parts of the Hamiltonian. Crucially, we complement the nonunitary dynamics of n_x by a constraint that maintains half-filling of the whole system at each point in time (note that, without the constraint, the wave function norm may both decrease and increase depending on the sign of $\text{Im} \mathcal{H}_{\text{meas}}^j$). The measurement in our formalism is thus the combined effect of the generalized (unitary + nonunitary) Hamiltonian dynamics and the projection onto the half-filling state that restores the norm of the state. This is analogous to measurement-induced quantum jumps [62] occurring with probabilities corresponding to local density measurements.

By construction, our formalism describes the evolution of the wave function conditioned on the measurement record (a particular sequence of “readouts” – random numbers m_x^j), and as such is suitable for the calculation of quantities like the entanglement entropy, which are not describable in terms of the Lindblad equation for the density matrix averaged over quantum trajectories. The emergence of an effective non-Hermitian Hamiltonian to describe the measurement process in conjunction with quantum jumps is an inherent part of the quantum trajectory approach [62, 63], with recent examples being Refs. [32, 33, 37, 39] for various choices of the effective Hamiltonians and jump operators. The fully “Hamiltonian”

nian” theoretical framework complements that of quantum circuits. Our model provides a conceptually particularly effective (and efficient) formalism to study the effect of measurement in the plane of two variables: the measurement rate (P) and the measurement strength (M), both encoded in Eq. (2).

It is worth noting that the measurement procedure induces correlations throughout the system, which travel with a velocity that is bounded from above. This is similar to the Lieb-Robinson bound; however, the maximum velocity in the presence of strong measurements is limited by M rather than by J . We thus require the discretization time step of the numerical integrator δt to satisfy $\delta t \ll \min\{M^{-1}, T\}$. This also clarifies the meaning of the term “continuous” when we refer above to the continuous restoration of the wave function norm—the restoration is discretized with the time step δt , which is the smallest time scale in the system.

Before we proceed in Sec. II C to describe the measurement protocol from the numerical perspective in more detail, let us comment on our choice of the initial state, which we take to be the ground state. As a starting point, we compute, using the density matrix renormalization group (DMRG), the ground state of the Hamiltonian (1). Time evolution is then implemented using the time-dependent variational principle (TDVP) [64], where we use the same hybrid approach as in Ref. [65], combining the one-site and two-site implementation of the TDVP. These methods are of the MPS class of algorithms, which are restricted to a variational subspace of the full Hilbert space, targeting low-entanglement states.

As a matter of principle, the MPS framework outlined above allows for a simulation of the crossover from weak to strong measurements for arbitrary interacting lattice Hamiltonians and arbitrary initial states. We opt to start the dynamics not from an unentangled product state, as is conventional, but from the ground state of the Hamiltonian (1). This has the following key advantage. The ground state is only moderately entangled, with a characteristic logarithmic scaling of entanglement entropy [10]. In the absence of measurements, the system remains in the ground state under unitary time evolution. Thus, any increase or reduction in entanglement is solely due to the measurement (and its interplay with \mathcal{H}_0). This should be contrasted with the case of an initial high-energy product state that rapidly entangles, reaching a volume-law entangled phase under the dynamics of \mathcal{H}_0 in the absence of any measurement. From a technical perspective, our choice of the initial condition speeds up the simulation of the dynamics, since a relatively modest size of the variational manifold suffices.

C. Protocol

We simulate the dynamics of the monitored chain governed by $\mathcal{H}_0 + \mathcal{H}_{\text{meas}}$, using various choices of measurement strength M , probability of measuring each site P ,

and system size L , in a time window $t \in [0, 50]$. We start from the ground state of \mathcal{H}_0 with $\Delta = -1/2$. We choose the measurement interval $T = 1$ and the time step $\delta t = 0.005$ for the TDVP integrator. At $t = 50$, we switch off the measurement Hamiltonian (2) and continue evolving according to the Hamiltonian (1) in a small time interval $t \in [50, 60]$. The size of the variational manifold is controlled by a numerical parameter called the bond dimension χ [59]. For finding the ground state we use $\chi = 500$, and for the dynamics we mainly use $\chi = 64$ (but for some values of L , P and M we benchmark our results using larger bond dimensions, see below). For each set of parameters, we repeat the procedure at least $R = 40$ times.

At each of the measurement steps $t = j = 0, 1, \dots$, we generate new measurement outcomes through the evolution of $n_x(t)$ and by taking new random numbers $m_x^{(j)}$. Hence, it is possible, depending on the dynamics and random chance, for one particular site to be measured as having a particle present, a hole present, or not being measured, and these outcomes can change during the time evolution. The dynamics under \mathcal{H}_0 alone tends to “delocalize” the system (a random product state will evolve towards a volume-law entangled state that is homogeneous in density), while the dynamics governed by $\mathcal{H}_{\text{meas}}$ rather tends to localize particles at the measured sites. We therefore expect a competition between both mechanisms that can potentially lead to a transition between delocalized (entangling) and localized (disentangling) types of behavior.

D. Comparison to existing approaches

Our protocol is aimed at mimicking the coupling to a measurement apparatus. The latter can be (on average) described by the Lindblad formalism using matrix product states (cf. Refs. [39, 61]). This can be viewed as a continuum analog of discrete quantum circuit models that have been studied recently (see Sec. I). Similarly, we are capable of following individual quantum trajectories without averaging over the measurement outcomes encoded in the sequence of random variables $m_x^{(j)}$. However, in contrast to random hybrid circuits, the unitary part of the evolution in our scheme is governed by the physical Hamiltonian of the system, and, hence, the “unitaries” applied to the site at consecutive time steps are not random but rather are determined by the same fixed (time-independent) Hamiltonian \mathcal{H}_0 . In addition, at each time step, we maintain half-filling, which provides a global constraint on the hybrid evolution of the system.

The way the local measurements are implemented is somewhat similar to the method employed in Refs. [34, 35] to describe non-interacting spin chains. The advantage of the current approach is that it permits the investigation of generic many-body systems on a lattice. A key difference between our approach and the MPS-

based approaches of Refs. [39, 61] is that in our protocol the “measurement” and the time evolution occur at the same time. Hence, there is a direct interplay between both aspects in the continuum time domain.

Our approach also bears some similarity to that in Ref. [37], where the quantum trajectory approach [62] was applied. In Ref. [37], exact diagonalization was employed, which is restricted to relatively small systems of $L \approx 20$. A continuous approach applied to random quantum circuits was also recently proposed in Ref. [16] where it was implemented for system sizes $L \leq 20$. There is also some similarity in spirit with the “quantum jump” algorithm used in the context of Monte Carlo simulations, as developed by Dalibard *et al.* [63]. In that algorithm, a stochastic element is introduced to model coupling of trapped dilute gases to an exterior electromagnetic field.

III. NUMERICAL RESULTS

In this section, we introduce the physical observables and the numerical results used to probe the entanglement transition.

A. Signatures of measurement-induced transition

1. Entanglement entropy

A measure that is useful as a diagnostic tool is the von Neumann entanglement entropy S [10]. An ergodic, thermalizing system is characterized by the volume-law growth of entanglement, whereas a localized system shows area-law growth of entanglement. In the case of a one-dimensional system, the volume law corresponds to a scaling $\propto L$, and the area law corresponds to just a constant. The von Neumann entropy of entanglement for a bipartition into subsystems A and B is given by:

$$S = -\text{Tr}(\rho_A \ln \rho_A), \quad \rho_A \equiv \text{Tr}_B |\Psi\rangle\langle\Psi|, \quad (3)$$

where ρ_A is the reduced density matrix of subsystem A .

The initial state we consider here—the ground state of a Luttinger liquid—has the feature that S is neither volume-law-entangled nor area-law-entangled, with S showing an intermediate behavior: a logarithmic growth with system size. This allows us to distinguish the entangling phase from the disentangling one by comparing the entropy after a sufficiently long time to the initial entropy. (Of course, strictly speaking, this requires the $L \rightarrow \infty$ limit, whereas in practice we are limited to large but finite L . The large- L requirement becomes particularly stringent close to the transition.) Below we calculate the time evolution of the entanglement entropy for individual quantum trajectories, as well as the entropy averaged over R runs.

Throughout this work, we measure the entropy S in units of $\ln 2$, which corresponds to a replacement $\ln \rightarrow \log_2$ in Eq. (3).

2. Particle density and clustering

Another useful—and experimentally accessible—measure is the particle density. In the limit of $M \gg 1$, “chokepoints” of high or low density (particles and holes) are generated that serve as blockades to correlations. It turns out to be instructive to consider the *cluster size*, which is a commonly used diagnostic tool in percolation transitions. Here we define a cluster as a set of consecutive sites with a density at most 0.2 from the extreme values (0 and 1). We then compute the maximum cluster length for each realization.

B. Simulations

1. Strong frequent measurement: $M \gg 1$, $P = 1$

First, we consider the case where measurement is strong, $M = 10$, and each site is always measured, $P = 1$. The results for the entanglement entropy and particle density are shown in Fig. 1. The entropy approaches zero on a time scale of order unity and remains very close to zero for the whole duration of the measurement run, with occasional spikes in the entropy representing rare fluctuations (“glitches”). The small, time-independent value of entropy clearly indicates that the system is characterized by the area-law scaling of entanglement, corresponding to the disentangling phase.

In terms of the density, a random configuration of particles and holes is chosen at the very beginning of each run, $t \sim 1$, and we observe the quantum Zeno effect [11]. The density profile in the x - t plane forms stripes of occupied and unoccupied states. Whether a given site is occupied or not is essentially determined by the random variable $m_x^{(j=1)}$ at the first step (so that there are no correlations between different sites). The pattern established at $t \sim 1$ remains almost unchanged at later times.

However, the particles are not exactly frozen: since M is finite, the dynamics driven by \mathcal{H}_0 slightly perturbs the product state, leading to a nonzero probability of a flip in the sign of $\mathcal{H}_{\text{meas}}$, as can be seen to occur in the Fig. 1. Nonetheless, long-range correlations are strongly suppressed and we observe an area-law state with essentially zero entanglement between distant parts of the system. A substantial entanglement appears only between neighbouring sites and only during the rare processes of particle hopping. When such flips occur close to the center of the system, where the bipartition is taken, they affect the entropy. This leads to rare peaks in the individual traces of $S(t)$ that lead to a finite value of entropy in the averages. Only in the limit $M \rightarrow \infty$, which corresponds to a projective measurement, does the quantum Zeno state become fully robust (i.e., strictly time-independent).

After switching off the measurement Hamiltonian, the density quickly settles to a homogeneous state (see the

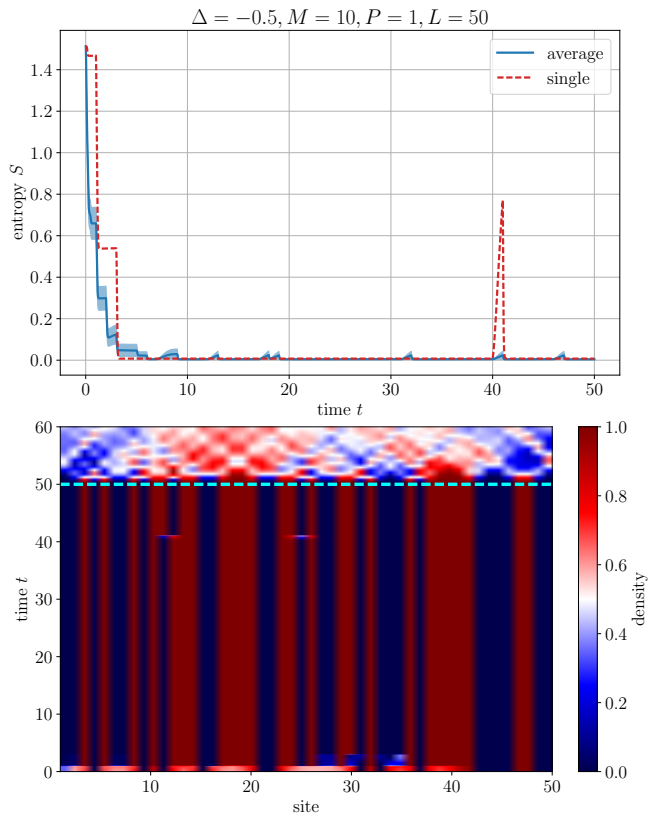


FIG. 1. Time evolution of the entropy S (top panel), showing the average over $R = 40$ realizations for $L = 50$, in the limit of strong frequent ($M = 10, P = 1$) measurement. The dashed red line corresponds to the entropy for an arbitrarily chosen single realization, with the corresponding density evolution in the bottom panel. The shaded area indicates a 1σ error, estimated through the standard deviation of $S(t)$ across the different realizations. The dashed line in the bottom panel indicates the time at which the measurement Hamiltonian (2) is switched off.

density plot above the dashed line in the lower panel of Fig. 1). The striped density pattern (appearing as an exact product state) at time $t = 50$ induces light-cone structures in the density evolution for $t > 50$. Since the energy of the measurement-stabilized striped phase is high, the entropy for $t > 50$ (not shown in Fig. 1) grows towards a volume-law value that is much higher than the initial one (that corresponded to a weakly entangled ground state of the Luttinger liquid, $S \propto \ln L$).

2. Strong infrequent measurement: $M \gg 1, P \ll 1$

Next, we consider the case where measurement is strong, as in the previous case, but the probability of measurement is much lower than unity. The result is shown in Fig. 2 for $M = 10$ and $P = 0.1$. In this case, the rare measurements do create locally polarized sites but they are not sufficient to suppress entanglement across

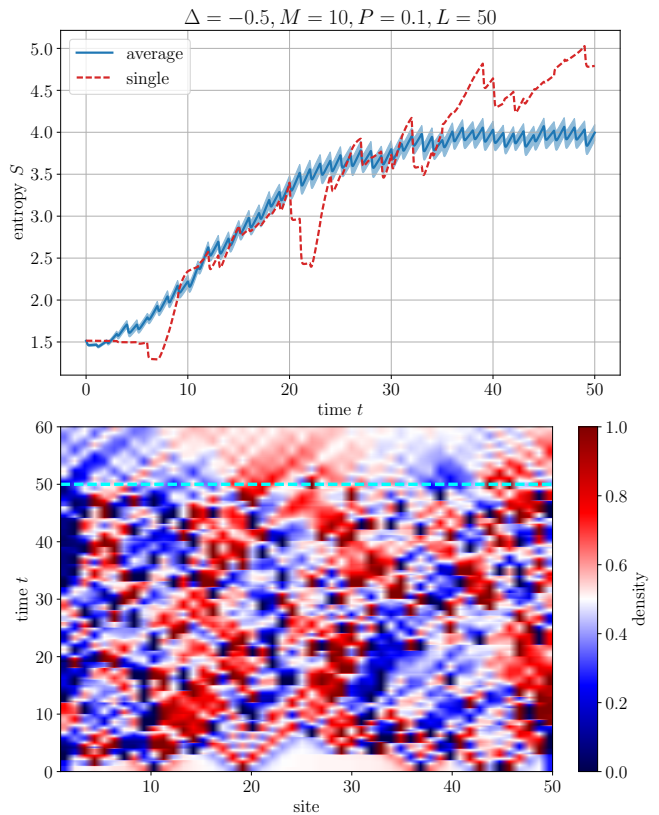


FIG. 2. Same as in Fig. 1, but for a strong infrequent ($M = 10, P = 0.1$) measurement. The initial density profile (local half-filling represented by the white color) develops into a random red-blue pattern on the time scale $t \sim 5$.

the system. On the contrary, the entanglement, while noisy, rapidly grows, reaching values substantially larger than the initial one. The system is thus in the entangling phase. The entanglement growth stems from quenching the system by the measurements that distort the initial homogeneous ground state by introducing rare polarized regions. These regions then develop in time according to the unitary dynamics governed by the many-body Hamiltonian (1).

As a result of this dynamics, the density becomes strongly inhomogeneous at later times; the inhomogeneity is further enhanced by subsequent rare strong measurements. Note that through the maintaining of global half-filling, local strong measurements affect neighboring sites: this can be clearly seen, e.g., at $t \sim 1$ around $x = 10$ and $x = 37$ in the lower panel of Fig. 2, where the projection on the globally-half-filled state induces an excess (reddish) density at the neighboring sites. We thus see that, under the global constraint in a realistic system, a local strong measurement can induce correlations, similar to non-local measurements [5, 26].

The zigzag fluctuation pattern in the average entropy on the scale of a single time step corresponds to the decrease in the entropy caused by the strong measurement in the vicinity of the bipartition cut. Eventually, the av-

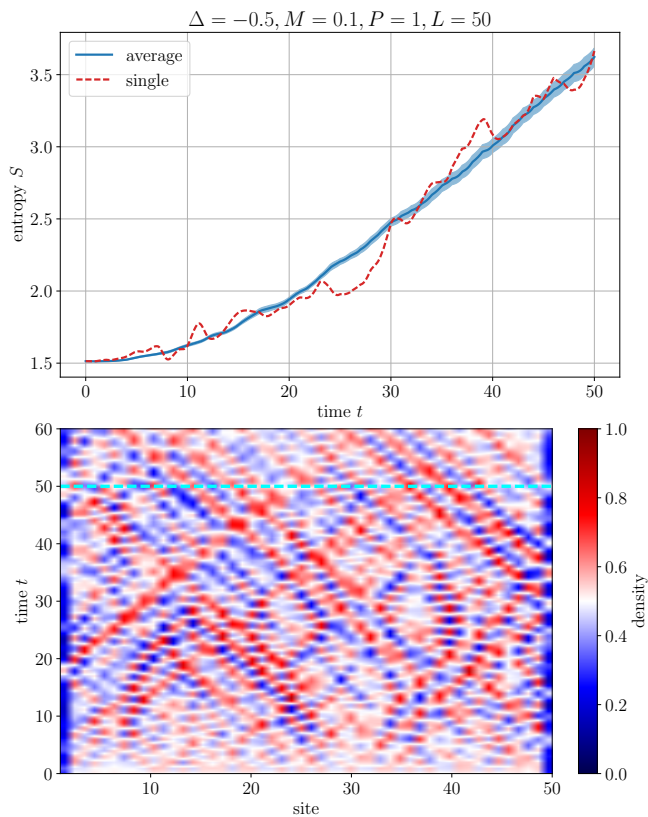


FIG. 3. Same as in Fig. 1, but for a weak frequent ($M = 0.1, P = 1$) measurement. Measurement-induced perturbations of the density propagate ballistically through the system and are reflected at the boundaries.

erage entropy saturates, as occasional decreases induced by the measurement and the entangling dynamics of the unitary Hamiltonian balance out, see Fig. 2.

3. Weak frequent measurement: $M \ll 1, P = 1$

We now consider the case where measurement is frequent but weak, see Fig. 3, where $P = 1$ and $M = 0.1$. In this case, the characteristic timescale for projecting onto a particle or hole state under the dynamics of $\mathcal{H}_{\text{meas}}$ is substantially larger than the timescale $T = 1$ associated with the duration of the measurement. This leads to a situation where the initial state, which has homogeneous density (except close to the edges of the system, in view of open boundary conditions) is only weakly perturbed by the measurement. As a result, we observe particle and hole fluctuations induced by the measurement, which traverse the system ballistically.

As seen in the upper panel of Fig. 3, the entanglement entropy rapidly grows with time and becomes considerably larger than its initial value, which is a signature of the entangling phase (see Sec. IV A 4). The physics of the entanglement growth can be understood as follows. The process of weak measurement continuously heats the

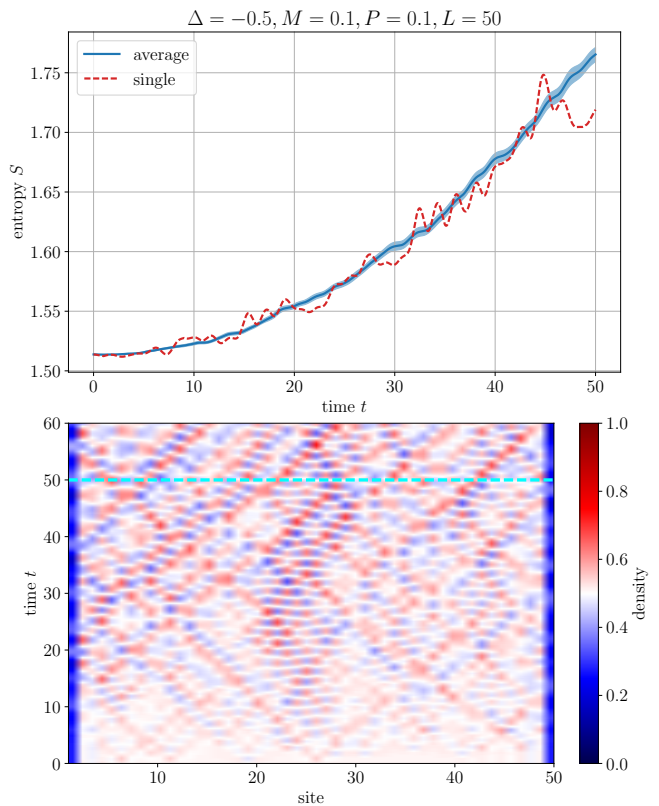


FIG. 4. Same as in Fig. 1, but for a weak infrequent ($M = 0.1, P = 0.1$) measurement.

system—the imaginary-time propagation does not conserve energy—and the system trends toward a highly entangled state at high energy, in qualitative similarity to the case of strong infrequent measurements depicted in Fig. 2. In the latter case, however, the heating (quenching) process is strongly inhomogeneous in space, whereas it is fairly uniform for a frequent, weak measurement. Consequently, the entropy curve shows a much smoother behavior.

4. Weak infrequent measurement: $M \ll 1, P \ll 1$

Finally, we consider the case where the measurement is both weak, $M = 0.1$, and infrequent, $P = 0.1$, see Fig. 4. This case is rather similar to the preceding one ($M \ll 1$ and $P = 1$, Sec. III B 3), except that the less frequent measurement naturally leads to less heating, so that the growth of the entropy is slower than in the case of frequent measurement. Nevertheless, the entanglement exhibits a clear growing trend, and the system is expected to eventually reach qualitatively the same, highly entangled high-energy state. Thus, at arbitrarily small values of M and P the entanglement will eventually grow to large values as the initial state at zero temperature is gradually heated by the (effective) coupling to the environment. Clearly, the time that is required for the entan-

gement to reach the saturation value becomes progressively longer when M and P are reduced.

The density pattern (lower panel of Fig. 4) is distorted already by a weak infrequent measurement, forming a structure of overlapping light-cone rays. Interestingly, the contrast appears to increase with time, which can be regarded as a result of the interplay between the unitary and measurement-induced dynamics: the measurements have a tendency to magnify density fluctuations.

IV. PHASE DIAGRAM

A. Entanglement entropy

We are now in a position to carry out a characterization of the dynamics of our monitored system in the parameter plane spanned by the measurement strength M and the measurement probability P . In section III B, we considered four limiting regimes corresponding to “corners” of this phase diagram. In the limit of large M and P , entanglement in the system is destroyed and an area-law phase appears. In the other three regimes, we found that entanglement *grows* with respect to the initial zero-temperature state because of the addition of energy to the system by measurements. Hence, we expect to find a transition between the two phases (disentangling and entangling) in the M – P plane. For hybrid quantum circuits, the phase diagram of this type was analyzed in Ref. [15], where the transition line connected two points, one located on the axis of weak constant measurement ($P = 1$) and the other corresponding to the limit of rare projective measurements ($M = \infty$).

1. Continuous measurements of all sites: constant $P = 1$

In Fig. 5a, we show the average entropy $S(t)$ for $P = 1$ and various choices of M from very weak ($M = 0.1$) to strong, nearly projective ($M = 10$) measurements. To probe the dependence of the entropy on the system size L , we compare in this plot the data for $L = 50$ and $L = 16$. For $L = 16$ we choose $\chi = 256$, so that the dynamics is simulated exactly (the exact simulation with MPS requires $\chi = 2^{L/2}$).

For large M , we see that the entropy decreases over time as was discussed in Sec. III B 1, which is consistent with the disentangling (area-law) phase. This is also confirmed by the fact that the long-time saturation value of S is independent on L (within the uncertainty that results from fluctuations of the average in our finite ensemble). Conversely, for small M , we see an increase of S with respect to its initial value as was discussed in Sec. III B 3. Furthermore, the entropy S increases with increasing system size L . These are hallmarks of the entangling phase. Our data indicate that the system is in the disentangling (area-law) phase for $M = 10, 3, 1$, and 0.5 , and in the

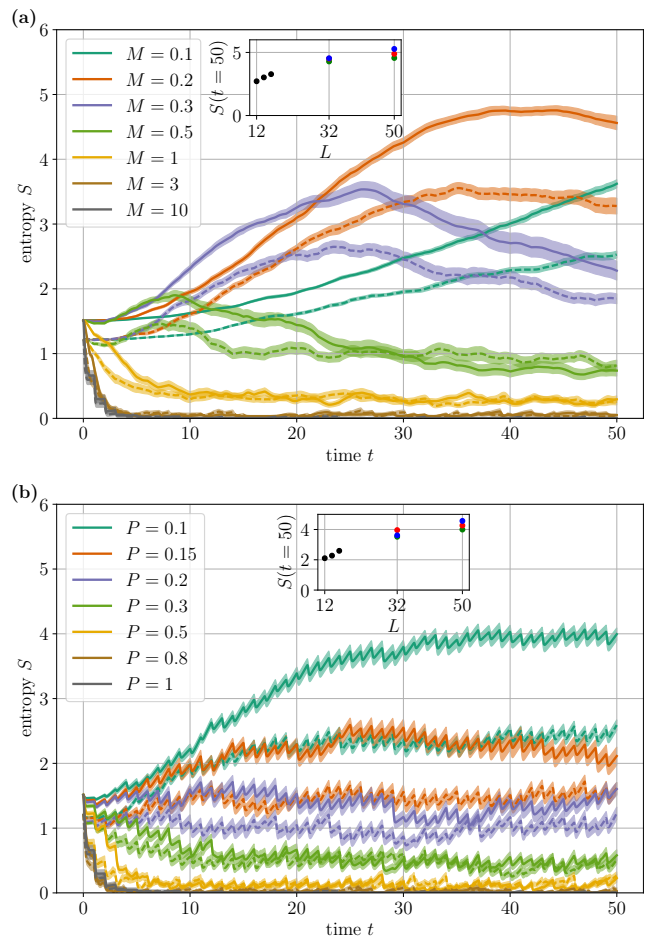


FIG. 5. **a)** Average entropy $S(t)$ as a function of time for various measurement strengths M and fixed $P = 1$. The solid (dashed) lines show $L = 50$ ($L = 16$). Inset: $S(t = 50)$ as a function of system size for $M = 0.2$, where exact results are shown for $L = 12, 14, 16$ and the colors indicate bond dimension for $L = 32, 50$, with $\chi = 64$ (green), $\chi = 96$ (red), $\chi = 128$ (blue). **b)** As in panel **a)**, but for fixed $M = 10$ and varying P . The inset shows results for $P = 0.1$.

entangling phase for $M = 0.1, 0.2$, and 0.3 . We thus estimate the position of the transition point on the $P = 1$ axis as $M_c \approx 0.4$.

Interestingly, for a certain range of values of M (see the curves for $M = 0.2, 0.3, 0.5$ in Fig. 5a), the entropy as a function of time exhibits a maximum before saturation. A similar effect was observed in Ref. [39] where, however, a very different initial condition was chosen (a high-energy, strongly inhomogeneous state, as opposed to the low-energy, homogeneous one considered here).

2. Strong measurements with varying measurement frequency: constant $M = 10$

In Fig. 5b, the time dependence of the average entropy $S(t)$ is shown for strong measurements. Specifically, in

this figure we fixed $M = 10$, while the measurement frequency P was varied from $P = 0.1$ to $P = 1$. Qualitatively, the evolution is quite similar to that shown in Fig. 5a. For small P , we find entangling behavior (Sec. III B 2), while for large P it is disentangling (Sec. III B 1). As in Fig. 5a, we have two complementary criteria for identification of the entangling phase: (i) the long-time value of the entropy is higher than its initial value; (ii) the entropy increases with system size ($L = 50$ vs $L = 16$). Both criteria yield consistent results, allowing us to identify the points $P = 1, 0.8, 0.5$, and 0.3 as belonging to the disentangling phase, and the points $P = 0.1, 0.15$, and 0.2 as belonging to the entangling phase, with the critical value being close to the latter point, $P_c \approx 0.2$ – 0.25 .

3. Overall phase diagram

In Fig. 6 we summarize the results for the entropy S , averaged over the time interval $[40, 50]$ and over $R = 40$ realizations, in the whole P – M parameter plane. In analogy with the above estimates of critical points on the $P = 1$ and $M = 10$ lines, we have estimated the transition line in the P – M plane, which is also shown in the figure.

It is worth commenting on the bottom left corner of the phase diagram (rare weak measurements), where the entropy is above its initial value but smaller than in the most of the entangling phase. The reason for this was discussed in Sec. III B 4: the entropy grows, but it takes a time much longer than the duration of the protocol to saturate (corresponding to a strongly entangled state).

4. Entropy scaling in the entangling phase

An important question is the dependence of the large- t saturation value of the entanglement entropy $S(L)$ on the system size L in the entangling phase. Most of works on entanglement transitions in quantum circuits indicate a volume-law scaling, $S(L) \propto L$, with a prefactor L depending on the measurement strength.

In the insets of Fig. 5 we show the behavior of the entropy at $t = 50$ as a function of system size, for two particular choices of parameters in the entangling phase ($M = 0.2, P = 1$ and $M = 10, P = 0.1$), which correspond to the largest values of S in the upper and lower panels of Fig. 5, respectively. For both these points in the parameter plane, saturation of the entropy as a function of time is reasonably reached by our largest time $t = 50$. In order to better quantify the rate of the entanglement growth, we have calculated the values of $S(t = 50)$ for these choices of P and M also for larger values of the bond dimension, $\chi = 96$ and 128 . For $L = 32$ the obtained values of the entropy for $\chi = 64$ and $\chi = 128$ are close in value (within statistical error bars that are related to a finite size of realizations and are of the order

of the symbol size), which is a signature of saturation of $S(t)$ with χ . At the same time, for $L = 50$ (where the entropy is larger), the obtained value of S for $\chi = 128$ is substantially above than that for $\chi = 64$. This drift indicates that, for these points in the P – M plane, the actual values of $S(t = 50)$ are still somewhat above the $\chi = 128$ results (shown by blue color in the insets); presumably by an amount of the order of a distance between the $\chi = 128$ and $\chi = 64$ points. (To find more accurately the saturated value, one would need a calculation with $\chi \approx 256$, which is in principle possible but requires very substantial computational time.) Keeping this in mind, we see that the values of the entanglement entropy at $L = 50$ are broadly consistent with volume-law trends based on the data for $L = 16$ and $L = 32$. We cannot exclude, however, a different type of scaling might emerge for larger system sizes or time scales.

It is worth noticing that the slopes of the $S(L)$ dependencies that can be estimated in this way are somewhat smaller than those that would be found based only on the data for small systems (accessible to exact diagonalization). This indicates that finite-size effects are sizeable, so that supplementing exact-diagonalization numerical studies by approximate approaches (such as the MPS method used in this work) that can be applied to larger systems is crucial.

The volume-law behavior of the entanglement entropy S in the entangling phase is also supported by the time dependence $S(t)$. In Fig. 7 we show the dependence $S(t)$ at $P = 1, M = 0.2$ for several system sizes (and for two values of the bond dimension χ for the largest sizes $L = 32$ and 50). We see that, for lengths $L \geq 24$, a linear increase $S(t) \propto t$ is found, with an L -independent slope. This is expected in the volume-law phase [13]: the entanglement increases as $S(t) \simeq sv_S t$ until it saturates at a time $t \simeq L/2v_S$ at a value $S(L) \simeq sL/2$, where v_S is the entanglement propagation velocity. When the bond dimension is insufficient, it leads to a cutoff of the linear increase of $S(t)$ and to the saturation before system-size effects kick in. The slope in Fig. 7 yields $sv_s \simeq 0.14$ for this point in the phase diagram. At the same time, the L -dependence of $S(L)$ in the inset of Fig. 5a yields an estimate $s = 2(dS/dL) \simeq 0.15 - 0.2$ for the same values of the parameters P and M . From these data, we estimate the entanglement propagation velocity, $v_S \equiv (sv_S)/s \simeq 0.7 - 1.0$. This velocity is close (or possibly identical) to the velocity of ballistic propagation of density fluctuations as observed, e.g., in Fig. 3, which is consistent with predictions from Refs. [8, 66].

It was proposed in Refs. [35, 36] that the volume-law scaling of $S(L)$ is only of transient character and crosses over to a $\ln L$ behavior for large L at the transition. The system sizes that we can access are not sufficient to rigorously test the validity of this conjecture.

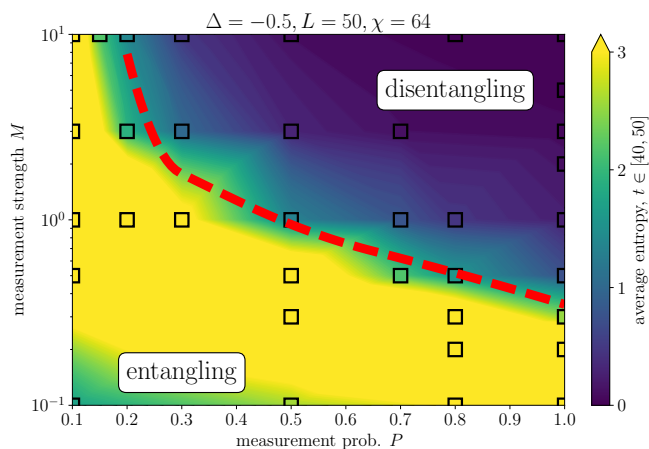


FIG. 6. Phase diagram, showing the averaged entropy S for $t \in [40, 50]$ for $R = 40$ realizations. The black squares indicate data points and the background color depicts interpolated values between the data points. The estimated phase boundary, corresponding to an approximate contour of constant entropy equal to the initial value, is shown as dashed red line.

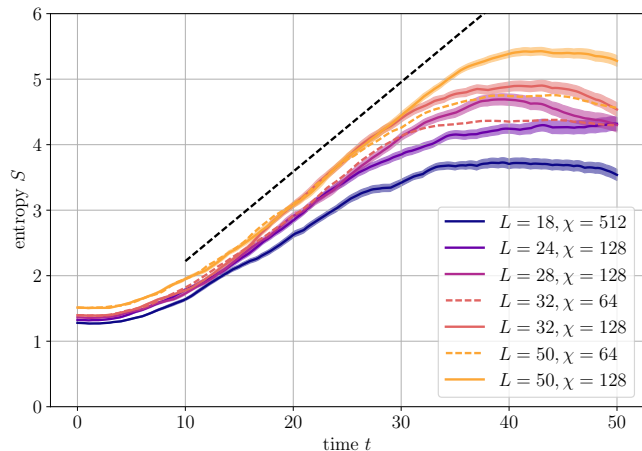


FIG. 7. Time dependence of the entanglement entropy $S(t)$ at $P = 1$, $M = 0.2$ for system sizes from $L = 18$ to $L = 50$. For the two largest system sizes, the data with bond dimensions $\chi = 64$ and 128 are shown, where $\chi = 64$ is indicated by a dashed line. The straight black dashed line is a guide to the eye obtained through a linear fit of the $L = 50$, $\chi = 128$ data in the linear regime $t \in [15, 30]$, yielding a slope ≈ 0.14 .

B. Clusterization

1. Clusterization at $\Delta = -0.5$

We discuss the clustering of particles (and holes), see Sec. III A 2. Interestingly, we observe, close to the transition from the disentangling to the entangling phase, the emergence of large domains resulting from the interplay of \mathcal{H}_0 and the measurement protocol. As an illustration, we show in Fig. 8 the dynamics for a single realization

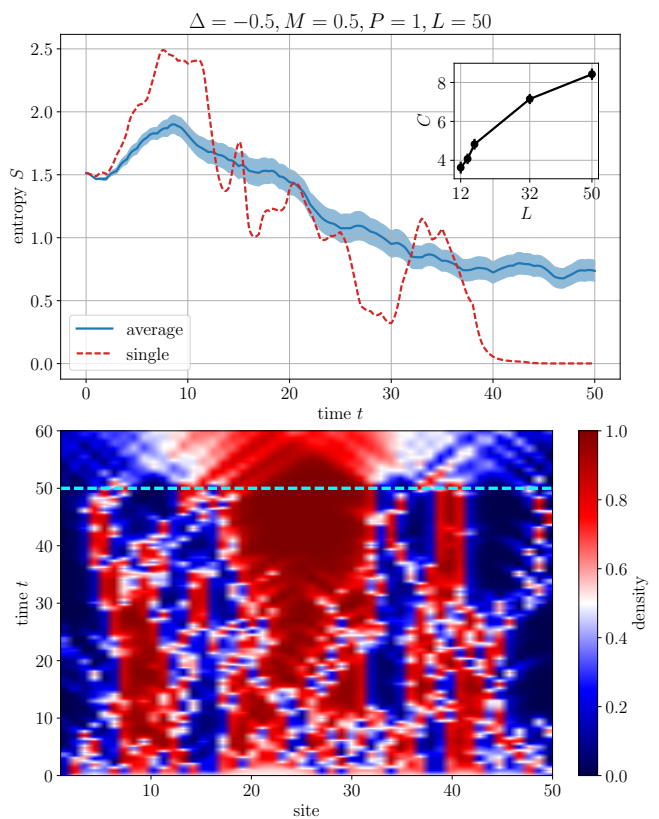


FIG. 8. As in Fig. 1, but for $M = 0.5$, $P = 1$. In the bottom panel, the realization with the largest maximum cluster size is chosen. Inset: average maximum cluster length C at $t = 50$ as a function of system size. Error bars indicate a 1σ -interval.

with $M = 0.5$ and $P = 1$. As discussed above, this point is on the area-law side of the transition, close to the phase boundary. For the single realization plotted in the lower panel—the one with the largest maximum cluster length—we observe formation of large polarized domains at time $t \approx 35$. As the dotted line in the upper panel shows, the entanglement entropy for this realization practically vanishes at $t \geq 40$. Hence, the large polarized regions effectively block transport, analogous to what is observed in models with local constraints [67].

To characterize the clustering quantitatively, we consider for every realization the maximum cluster length and then average it over all realizations. The resulting averaged maximum cluster length is denoted $C(t)$. In the inset of Fig. 8, we show the system-size dependence of $C(t = 50)$ for the same parameters $M = 0.5$, $P = 1$. A clear increase of C with system size L is observed. The data suggests sublinear growth $C \sim L^y$, with $y \approx 0.5$. The results for $C(t = 50)$ for various values of P and M are shown in Fig. 9. They exhibit a peak—which reveals the clusterization phenomenon—on the right side of the diagram, around the phase boundary between the entangling and disentangling phases. It should be emphasized that this clusterization is observed only near the portion of the phase boundary that corresponds to frequent mea-

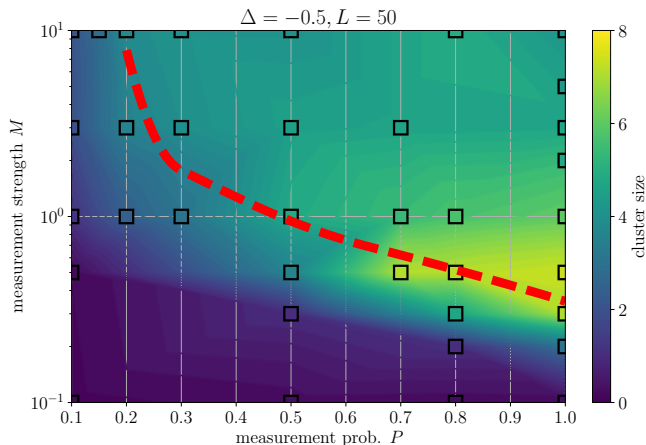


FIG. 9. Average maximum cluster length as a function of measurement probability P and measurement strength M , evaluated at $t = 50$. Note that the region with high cluster size is located around a section of the phase boundary between entangling and disentangling phases (Fig. 6), which is also shown in this plot.

measurements (P close to unity). No such peak is observed in the opposite corner of the phase diagram. This indicates that at least some important aspects of the entanglement transition are not fully universal and, in particular, differ qualitatively between the regimes of weak and strong measurements.

Clusterization can be viewed as a result of an enhancement of the attractive interaction by coupling of the system to the environment via the measurements, cf. Ref. [36]). As shown in the following section, the clusterization effect exists (in a weaker form) also in a non-interacting system ($\Delta = 0$), where the measurements create an effective attractive interaction. One can also note a certain similarity between the clustering and the dynamical quantum Zeno transition [32, 68]. Indeed, the rapid emergence of clusterization in the lower panel of Fig. 8 at $t \approx 35$ suggests a kind of dynamical phase transition induced by constantly monitoring the system at moderately weak measurement strength.

Qualitatively, one can understand the clusterization phenomenon as follows. Upon measuring a certain spatial region, an extended fluctuation may emerge, where the density is, e.g., increased compared to the background (the overall half-filling condition is then maintained at the expense of distant regions). The unitary dynamics leads to a spreading of this density seed to neighbouring sites, which are then more likely to have a higher density in the subsequent time evolution. For not too weak measurements, the “contrast” of the density fluctuation is enhanced by the measurement back-action. Over time, this leads to clusters of particles (or holes) with similar density. This can be dubbed a “dynamical quantum Zeno effect.”

It is no surprise that this phenomenon requires the measurement and unitary parts of the Hamiltonian to

be of roughly equal importance, as is the case near the crossover from the disentangling to entangling regime. After all, for $M \gg 1$ the unitary dynamics plays almost no role and sites are effectively locked at a fixed filling (a static quantum Zeno effect), with only occasional “jumps.” This results in freezing the striped structure of the density with a random distribution of the stripe sizes determined by the outcome of the first measurements, cf. Fig. 1, without any preference to increased clusters. The measurement also needs to be sufficiently frequent, otherwise the density correlations will be lost during the unitary time evolution. In the limit $M \ll 1$ the measurement can be considered only a weak perturbation that acts as a local heating process. Similarly, if $P \ll 1$ it is unlikely that neighboring sites are measured. Since the spreading of the density fluctuations to neighbouring sites is driven by the hopping term J , we expect only a modest effect of interactions on clusterization, which is confirmed in the following section.

2. Role of interactions

We proceed by discussing the role of interaction in the clusterization phenomenon. In the vicinity of the entanglement-transition phase boundary (in the regime of frequent, intermediate-strength measurements), the measurement effectively enhances the ferromagnetic interaction, which shows up in the clusterization, as discussed above. A natural question to ask is what the role of interaction is in this phenomenon. If the measurement can effectively enhance the interaction, then perhaps it can also create an effective interaction in an otherwise non-interacting system? To test this hypothesis, we have performed the analysis for a non-interacting system ($\Delta = 0$) that has otherwise the same parameters as in Fig. 8, i.e., $M = 0.5$, $P = 1$ (which are close to the point where the maximum degree of clusterization for the interacting system is observed). The results shown in Fig. 10 illustrate an enhanced clusterization that is indeed observed also for a non-interacting system. At the same time, the average maximum cluster size over $R = 40$ realizations, $C = 7.15 \pm 0.28$, turns out to be lower than for the interacting system (see inset of Fig. 8), as expected.

For values of the interaction $|\Delta| > 1$, the ground state of the system is ferromagnetic (for $\Delta < -1$) or antiferromagnetic (for $\Delta > 1$). A typical simulation for the antiferromagnetic case is shown in Fig. 11 for $\Delta = 1.5$. One sees that the system still develops clusters, counteracting the antiferromagnetic correlations. The inset in Fig. 11 shows C as a function of interaction strength for $L = 50$, confirming that clusterization is enhanced by attractive interactions. Within the regime $|\Delta| < 1$, we find a modest but statistically significant growth of the cluster size for attractive interactions, while C is constant within error bars in the repulsive regime $0 < \Delta < 1$. In the ferromagnetic regime (not shown in the figure), the initial

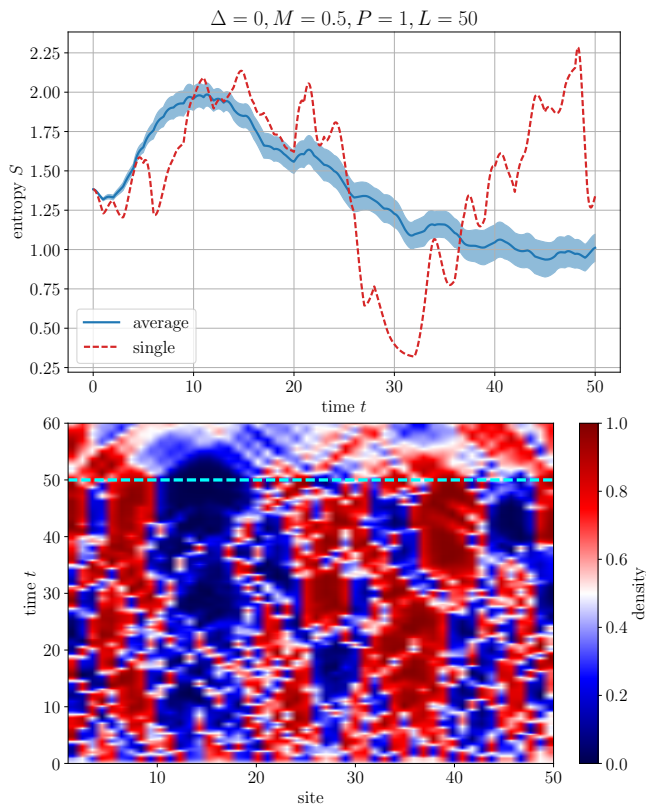


FIG. 10. As in Fig. 1, but for $M = 0.5$, $P = 1$ and $\Delta = 0$, such that the system is non-interacting.

state already has a cluster of $L/2$ particles, which is maintained during time evolution, yielding $C = 24.85 \pm 0.06$ using $\Delta = -1.5$.

V. SUMMARY AND DISCUSSION

In conclusion, we have proposed an MPS-based method for simulation of the dynamics of quantum many-body systems under continuous monitoring. The monitoring process is modelled as a site- and time-dependent non-Hermitian term in the Hamiltonian. The measurement protocol is controlled by two key parameters: the probability P that a given site is measured at a given time interval (with $0 < P \leq 1$) and the measurement strength M (with $M \ll 1$ corresponding to weak measurement and $M \gg 1$ to strong, nearly projective measurement). In contrast to recent approaches, our protocol starts from the ground state of the original Hamiltonian, so that the observed evolution of the initial state is entirely due to the effect of the measurements (including, of course, the interplay with the unitary dynamics).

We have applied the method to a 1D interacting many-body system, the ground state of which is a Luttinger liquid with a moderate entanglement ($S \propto \ln L$). The local measurement induces two competing processes: sufficiently strong measurements tend to disentangle the sys-

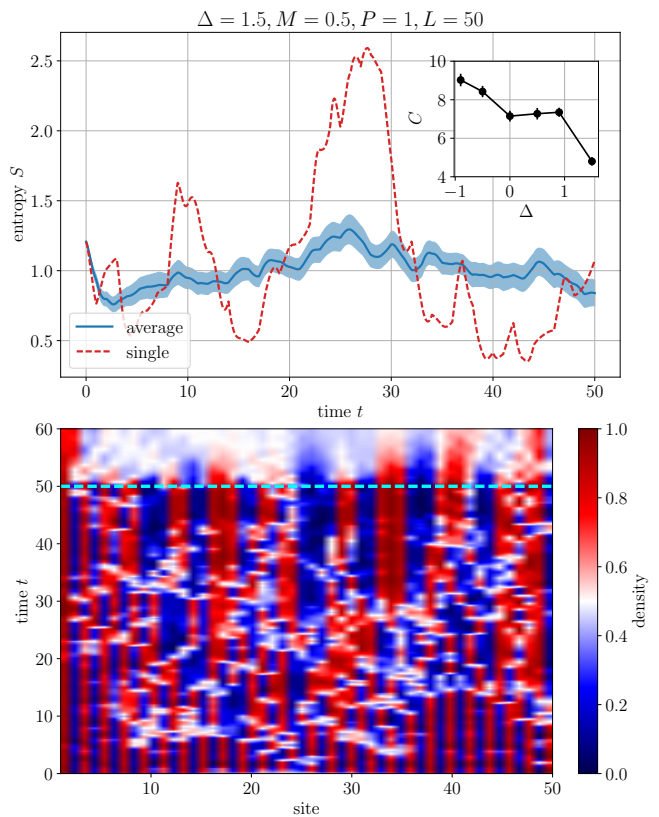


FIG. 11. As in Fig. 1, but for $M = 0.5$, $P = 1$ and $\Delta = 1.5$, such that the dynamics starts from an antiferromagnetic ground state. Inset: average maximum cluster length C as a function of interaction strength Δ for $L = 50$, evaluated at $t = 50$. Error bars are 1σ -intervals.

tem through quasi-projections. At the same time, the measurement also leads to effective local heating of the initial zero-temperature ground state, which can lead to stronger entanglement. If the measurement leads to an area-law (disentangling) phase, it reduces the entanglement entropy with respect to the initial state (in the limit of large L). On the other hand, if the measurement drives the system to the volume-law (entangling) phase, it enhances the entanglement entropy compared to the initial state. Note that the competing effects of measurement reported in Ref. [26] involve nonlocal measurements, as opposed to our protocol.

Exploring systems with a length up to $L = 50$, we have determined the phase diagram of the entanglement transition in the P - M plane (Fig. 6). For sufficiently strong and at the same time sufficiently frequent measurement (as in Fig. 1), we find a disentangling phase: the entanglement entropy gets suppressed by measurement down to an L -independent value (area law). On the other hand, if the measurement is sufficiently weak and/or sufficiently rare (as in Figs. 2, 3, and 4), the system is in the entangling phase. Our results for the entanglement entropy in this phase are consistent, for the system sizes studied, with a volume law ($S \propto L$). The obtained phase

diagram of the entanglement transition for the Hamiltonian system is qualitatively similar to earlier results for quantum circuits. Our findings thus indicate that such entangling-to-disentangling transitions occur generically in quantum many-body systems.

Furthermore, we find that, close to the phase boundary in the range of frequent measurements ($P \approx 1$), the entanglement transition is accompanied by an increase of the size of clusters of particles and holes (Figs. 8 and 9). We interpret this phenomenon as an enhancement of the attractive interaction by the measurements. A similar phenomenon, although in a somewhat weaker form, is found also for a non-interacting system. The divergence of cluster size close to the entanglement transition may be a useful experimental probe, since particle densities are generally easier to measure than the entanglement entropy. Indeed, a setup similar to the one described in this work may be readily prepared in experiments on ultracold atoms or trapped ions, as the local particle density can be measured using quantum microscopy [69]. It is an intriguing possibility that the divergence of cluster size we observe could be a signature of a transition to a dynamical quantum Zeno phase (cf. Ref. [32]). At the same time, the precise connection between the clusterization effect and the measurement transition remains to be clarified.

Future work may focus on applying the method outlined here to various models of experimental relevance, such as the Hubbard model. An experimental implementation of the open quantum Ising chain on IBM's quantum hardware was realized very recently [70].

ACKNOWLEDGMENTS

We thank M. Buchhold, S. Diehl, A. Romito, S. Roy, K. Snizhko and M. Szyniszewski for useful discussions. Numerical simulations were performed using the TeNPy library (version 0.6.1) [71]. We acknowledge financial support from the Deutsche Forschungsgemeinschaft (DFG): Project No. 277101999 – TRR 183 (Project C01) and Grants No. EG 96/13-1 and No. GO 1405/6-1, as well as from the Israel Science Foundation.

Appendix A: Numerical details and convergence

The numerical method outlined in the main text employs MPS [59] to simulate pure states. The key numeri-

cal convergence parameter is the bond dimension, which controls the size of the variational manifold. Deep in the entangling regime, we have shown that the entanglement grows rapidly, as expected, leading to eventual cutoff effects due to bond dimension truncation (see Fig. 7).

Let us consider the situation around the border between the observed disentangling and entangling regimes, in the region where we observe a peak in clusterization. We therefore take $L = 50$, $P = 1$ and $M = 0.5$. The results are shown in Fig. 12. As estimated for the maximum cluster size at $t = 50$ we obtain $C = 8.43 \pm 0.29$ for $\chi = 64$ and $C = 8.18 \pm 0.28$ for $\chi = 128$ (with 1σ error bars), so that the results converged with bond dimension. Moreover, we can see that the curves for the average entropy match within error bars. Note that, since the measurement Hamiltonian (2) explicitly depends on the many-body wave function itself and has a stochastic character, it is not possible to simulate exactly the same measurement outcomes. Thus, some small differences related to these random fluctuations remain even though convergence with the bond dimension is reached.

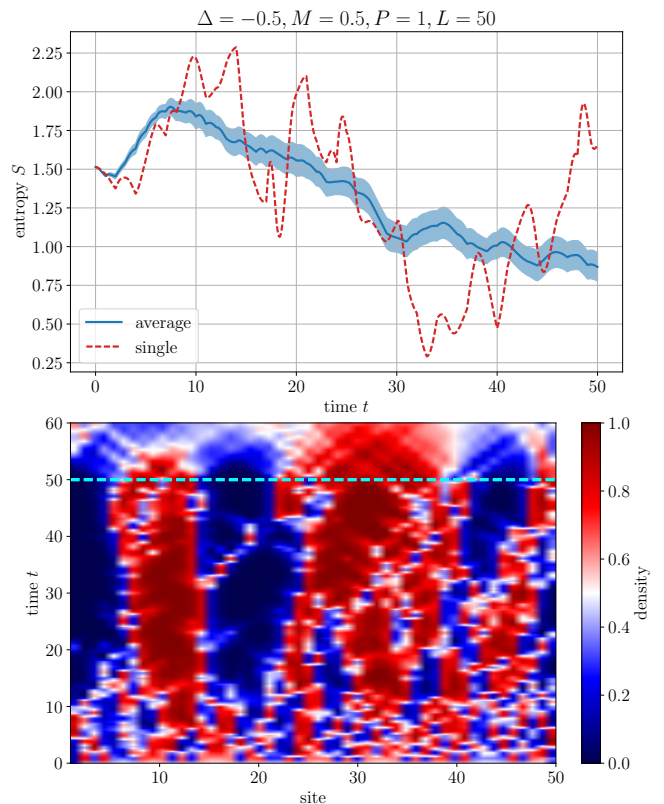


FIG. 12. As in Fig. 8, but for $\chi = 128$. In the bottom panel, the realization with the largest cluster size is chosen.

[1] H.-P. Breuer and F. Petruccione, *The theory of open quantum systems* (Oxford University Press, Oxford,

2002).

[2] I. Rotter and J. P. Bird, A review of progress in the

- physics of open quantum systems: theory and experiment, *Rep. Prog. Phys.* **78**, 114001 (2015).
- [3] A. Polkovnikov, K. Sengupta, A. Silva, and M. Vengalattore, Colloquium: Nonequilibrium dynamics of closed interacting quantum systems, *Rev. Mod. Phys.* **83**, 863 (2011).
- [4] F. Arute *et al.*, Quantum supremacy using a programmable superconducting processor, *Nature* **574**, 505 (2019).
- [5] S. Roy, J. T. Chalker, I. V. Gornyi, and Y. Gefen, Measurement-induced steering of quantum systems, *Phys. Rev. Research* **2**, 033347 (2020).
- [6] M. Schlosshauer, Decoherence, the measurement problem, and interpretations of quantum mechanics, *Rev. Mod. Phys.* **76**, 1267 (2005).
- [7] H. M. Wiseman and G. J. Milburn, *Quantum Measurement and Control* (Cambridge University Press, Cambridge (UK), 2009).
- [8] P. Calabrese and J. Cardy, Entanglement entropy and quantum field theory, *J. Stat. Mech.: Theory Exp.* **2004** (06), P06002.
- [9] R. Horodecki, P. Horodecki, M. Horodecki, and K. Horodecki, Quantum entanglement, *Rev. Mod. Phys.* **81**, 865 (2009).
- [10] N. Laflorencie, Quantum entanglement in condensed matter systems, *Phys. Rep.* **646**, 1 (2016).
- [11] Y. Li, X. Chen, and M. P. A. Fisher, Quantum Zeno effect and the many-body entanglement transition, *Phys. Rev. B* **98**, 205136 (2018).
- [12] A. Chan, R. M. Nandkishore, M. Pretko, and G. Smith, Unitary-projective entanglement dynamics, *Phys. Rev. B* **99**, 224307 (2019).
- [13] B. Skinner, J. Ruhman, and A. Nahum, Measurement-induced phase transitions in the dynamics of entanglement, *Phys. Rev. X* **9**, 031009 (2019).
- [14] Y. Li, X. Chen, and M. P. A. Fisher, Measurement-driven entanglement transition in hybrid quantum circuits, *Phys. Rev. B* **100**, 134306 (2019).
- [15] M. Szyniszewski, A. Romito, and H. Schomerus, Entanglement transition from variable-strength weak measurements, *Phys. Rev. B* **100**, 064204 (2019).
- [16] M. Szyniszewski, A. Romito, and H. Schomerus, Universality of entanglement transitions from stroboscopic to continuous measurements, *Phys. Rev. Lett.* **125**, 210602 (2020).
- [17] Y. Bao, S. Choi, and E. Altman, Theory of the phase transition in random unitary circuits with measurements, *Phys. Rev. B* **101**, 104301 (2020).
- [18] M. J. Gullans and D. A. Huse, Dynamical purification phase transition induced by quantum measurements, *Phys. Rev. X* **10**, 041020 (2020).
- [19] C.-M. Jian, Y.-Z. You, R. Vasseur, and A. W. W. Ludwig, Measurement-induced criticality in random quantum circuits, *Phys. Rev. B* **101**, 104302 (2020).
- [20] C.-M. Jian, B. Bauer, A. Keselman, and A. W. W. Ludwig, Criticality and entanglement in non-unitary quantum circuits and tensor networks of non-interacting fermions (2020), [arXiv:2012.04666 \[cond-mat.stat-mech\]](https://arxiv.org/abs/2012.04666).
- [21] S. Choi, Y. Bao, X.-L. Qi, and E. Altman, Quantum error correction in scrambling dynamics and measurement-induced phase transition, *Phys. Rev. Lett.* **125**, 030505 (2020).
- [22] R. Fan, S. Vijay, A. Vishwanath, and Y.-Z. You, Self-organized error correction in random unitary circuits with measurement, *Phys. Rev. B* **103**, 174309 (2021).
- [23] X. Chen, Y. Li, M. P. A. Fisher, and A. Lucas, Emergent conformal symmetry in nonunitary random dynamics of free fermions, *Phys. Rev. Research* **2**, 033017 (2020).
- [24] S. Sang and T. H. Hsieh, Measurement-protected quantum phases, *Phys. Rev. Research* **3**, 023200 (2021).
- [25] A. Zabalo, M. J. Gullans, J. H. Wilson, S. Gopalakrishnan, D. A. Huse, and J. H. Pixley, Critical properties of the measurement-induced transition in random quantum circuits, *Phys. Rev. B* **101**, 060301(R) (2020).
- [26] M. Ippoliti, M. J. Gullans, S. Gopalakrishnan, D. A. Huse, and V. Khemani, Entanglement phase transitions in measurement-only dynamics, *Phys. Rev. X* **11**, 011030 (2021).
- [27] A. Lavasani, Y. Alavirad, and M. Barkeshli, Measurement-induced topological entanglement transitions in symmetric random quantum circuits, *Nat. Phys.* **17**, 342–347 (2021).
- [28] M. Ippoliti and V. Khemani, Postselection-free entanglement dynamics via spacetime duality, *Phys. Rev. Lett.* **126**, 060501 (2021).
- [29] O. Lunt and A. Pal, Measurement-induced entanglement transitions in many-body localized systems, *Phys. Rev. Research* **2**, 043072 (2020).
- [30] N. Lang and H. P. Büchler, Entanglement transition in the projective transverse field Ising model, *Phys. Rev. B* **102**, 094204 (2020).
- [31] D. Rossini and E. Vicari, Measurement-induced dynamics of many-body systems at quantum criticality, *Phys. Rev. B* **102**, 035119 (2020).
- [32] A. Biella and M. Schiró, Many-body quantum Zeno effect and measurement-induced subradiance transition (2021), [arXiv:2011.11620 \[quant-ph\]](https://arxiv.org/abs/2011.11620).
- [33] X. Turkeshi, A. Biella, R. Fazio, M. Dalmonte, and M. Schiró, Measurement-induced entanglement transitions in the quantum Ising chain: From infinite to zero clicks, *Phys. Rev. B* **103**, 224210 (2021).
- [34] X. Cao, A. Tilloy, and A. D. Luca, Entanglement in a fermion chain under continuous monitoring, *SciPost Phys.* **7**, 24 (2019).
- [35] O. Albertson, M. Buchhold, and S. Diehl, Entanglement transition in a monitored free-fermion chain: From extended criticality to area law, *Phys. Rev. Lett.* **126**, 170602 (2021).
- [36] M. Buchhold, Y. Minoguchi, A. Altland, and S. Diehl, Effective theory for the measurement-induced phase transition of Dirac fermions (2021), [arXiv:2102.08381 \[cond-mat.stat-mech\]](https://arxiv.org/abs/2102.08381).
- [37] Y. Fuji and Y. Ashida, Measurement-induced quantum criticality under continuous monitoring, *Phys. Rev. B* **102**, 054302 (2020).
- [38] T. Minato, K. Sugimoto, T. Kuwahara, and K. Saito, Fate of measurement-induced phase transition in long-range interactions (2021), [arXiv:2104.09118 \[quant-ph\]](https://arxiv.org/abs/2104.09118).
- [39] S. Goto and I. Danshita, Measurement-induced transitions of the entanglement scaling law in ultracold gases with controllable dissipation, *Phys. Rev. A* **102**, 033316 (2020).
- [40] K. Snizhko, P. Kumar, N. Rao, and Y. Gefen, Weak-measurement-induced asymmetric dephasing: a topological transition (2020), [arXiv:2006.13244 \[quant-ph\]](https://arxiv.org/abs/2006.13244).
- [41] K. Snizhko, N. Rao, P. Kumar, and Y. Gefen, Weak-measurement-induced phases and dephasing: broken symmetry of the geometric phase (2020),

- arXiv:2006.14641 [quant-ph].
- [42] P. Kumar, K. Snizhko, and Y. Gefen, Engineering two-qubit mixed states with weak measurements, *Phys. Rev. Research* **2**, 042014 (R) (2020).
- [43] V. Gebhart, K. Snizhko, T. Wellens, A. Buchleitner, A. Romito, and Y. Gefen, Topological transition in measurement-induced geometric phases, *Proc. Natl. Acad. Sci. U.S.A.* **117**, 5706 (2020).
- [44] L. Xu, Z. Liu, A. Datta, G. C. Knee, J. S. Lundeen, Y.-q. Lu, and L. Zhang, Approaching quantum-limited metrology with imperfect detectors by using weak-value amplification, *Phys. Rev. Lett.* **125**, 080501 (2020).
- [45] D. A. Ivanov, T. Y. Ivanova, S. F. Caballero-Benitez, and I. B. Mekhov, Feedback-induced quantum phase transitions using weak measurements, *Phys. Rev. Lett.* **124**, 010603 (2020).
- [46] J. Manousakis, C. Wille, A. Altland, R. Egger, K. Flensberg, and F. Hassler, Weak measurement protocols for Majorana bound state identification, *Phys. Rev. Lett.* **124**, 096801 (2020).
- [47] M. H. Muñoz Arias, P. M. Poggi, P. S. Jessen, and I. H. Deutsch, Simulating nonlinear dynamics of collective spins via quantum measurement and feedback, *Phys. Rev. Lett.* **124**, 110503 (2020).
- [48] J. T. Monroe, N. Yunger Halpern, T. Lee, and K. W. Murch, Weak measurement of a superconducting qubit reconciles incompatible operators, *Phys. Rev. Lett.* **126**, 100403 (2021).
- [49] Y. Wang, K. Snizhko, A. Romito, Y. Gefen, and K. Murch, Observing a topological transition in weak-measurement-induced geometric phases (2021), arXiv:2102.05660 [quant-ph].
- [50] M. Van Regemortel, Z.-P. Cian, A. Seif, H. Dehghani, and M. Hafezi, Entanglement entropy scaling transition under competing monitoring protocols, *Phys. Rev. Lett.* **126**, 123604 (2021).
- [51] M. J. Gullans and D. A. Huse, Scalable probes of measurement-induced criticality, *Phys. Rev. Lett.* **125**, 070606 (2020).
- [52] S. Sang, Y. Li, T. Zhou, X. Chen, T. H. Hsieh, and M. P. A. Fisher, Entanglement negativity at measurement-induced criticality (2020), arXiv:2012.00031 [cond-mat.stat-mech].
- [53] Y. Li and M. P. A. Fisher, Statistical mechanics of quantum error correcting codes, *Phys. Rev. B* **103**, 104306 (2021).
- [54] Y. Bao, S. Choi, and E. Altman, Symmetry enriched phases of quantum circuits (2021), arXiv:2102.09164 [cond-mat.stat-mech].
- [55] Y. Li, X. Chen, A. W. W. Ludwig, and M. P. A. Fisher, Conformal invariance and quantum non-locality in hybrid quantum circuits (2020), arXiv:2003.12721 [quant-ph].
- [56] P. Calabrese and J. Cardy, Entanglement entropy and conformal field theory, *J. Phys. A* **42**, 504005 (2009).
- [57] S.-K. Jian, C. Liu, X. Chen, B. Swingle, and P. Zhang, SYK meets non-hermiticity ii: measurement-induced phase transition (2021), arXiv:2104.08270 [cond-mat.str-el].
- [58] S. Gopalakrishnan and M. J. Gullans, Entanglement and purification transitions in non-hermitian quantum mechanics, *Phys. Rev. Lett.* **126**, 170503 (2021).
- [59] U. Schollwöck, The density-matrix renormalization group in the age of matrix product states, *Ann. Phys. (N. Y.)* **326**, 96 (2011).
- [60] S. Paeckel, T. Köhler, A. Swoboda, S. R. Manmana, U. Schollwöck, and C. Hubig, Time-evolution methods for matrix-product states, *Ann. Phys. (N. Y.)* **411**, 167998 (2019).
- [61] Q. Tang and W. Zhu, Measurement-induced phase transition: A case study in the nonintegrable model by density-matrix renormalization group calculations, *Phys. Rev. Research* **2**, 013022 (2020).
- [62] A. J. Daley, Quantum trajectories and open many-body quantum systems, *Adv. Phys.* **63**, 77 (2014).
- [63] J. Dalibard, Y. Castin, and K. Mølmer, Wave-function approach to dissipative processes in quantum optics, *Phys. Rev. Lett.* **68**, 580 (1992).
- [64] J. Haegeman, C. Lubich, I. Oseledets, B. Vandereycken, and F. Verstraete, Unifying time evolution and optimization with matrix product states, *Phys. Rev. B* **94**, 165116 (2016).
- [65] E. V. H. Doggen, I. V. Gornyi, A. D. Mirlin, and D. G. Polyakov, Slow many-body delocalization beyond one dimension, *Phys. Rev. Lett.* **125**, 155701 (2020).
- [66] G. De Chiara, S. Montangero, P. Calabrese, and R. Fazio, Entanglement entropy dynamics of Heisenberg chains, *J. Stat. Mech.: Theory Exp.* **2006**, P03001.
- [67] E. V. H. Doggen, I. V. Gornyi, and D. G. Polyakov, Stark many-body localization: Evidence for Hilbert-space shattering, *Phys. Rev. B* **103**, L100202 (2021).
- [68] K. Snizhko, P. Kumar, and A. Romito, Quantum Zeno effect appears in stages, *Phys. Rev. Research* **2**, 033512 (2020).
- [69] W. S. Bakr, J. I. Gillen, A. Peng, S. Fölling, and M. Greiner, A quantum gas microscope for detecting single atoms in a Hubbard-regime optical lattice, *Nature* **462**, 74 (2009).
- [70] H. Kamakari, S.-N. Sun, M. Motta, and A. J. Minnich, Digital quantum simulation of open quantum systems using quantum imaginary time evolution (2021), arXiv:2104.07823 [quant-ph].
- [71] J. Hauschild and F. Pollmann, Efficient numerical simulations with Tensor Networks: Tensor Network Python (TeNPy), *SciPost Phys. Lect. Notes*, **5** (2018), code available from <https://github.com/tenpy/tenpy>.